Size-Dependent Adsorption Performance of ZnO Nanoclusters for Drug Delivery Applications

Mustafa Kurban (mkurbanphys@gmail.com)
Ahi Evran Universitesi Muhendislik Mimarlik Fakultesi https://orcid.org/0000-0002-7263-0234
İskender Muz
Nevşehir Hacı Bektaş Veli Üniversitesi: Nevsehir Haci Bektas Veli Universitesi

Research Article

Keywords: ZnO Nanoclusters, Favipiravir, Adsorption, DFT, Drug delivery

Posted Date: May 23rd, 2022

DOI: https://doi.org/10.21203/rs.3.rs-1607402/v1

Abstract

We have investigated the size-dependent adsorption performance of ZnO nanoclusters (NCs) as drug delivery carriers for the first time. Our results show that the adsorption energy of the favipiravir drug on the ZnO NCs is predicted in the range of -26.69 kcal/mol and − 34.27 kcal/mol. The adsorption energy (-34.27 kcal/mol) between $(ZnO)_{18}$ NC and the favipiravir is energetically desirable and more favorable than the other interactions. The size of ZnO NCs and the position of the favipiravir on the ZnO NCs cause a decrease in the energy gap, which makes the charge-transfer process easier. The bonds between O – Zn, N – Zn and F – Zn atoms exhibit dual covalent and ionic natures. The non-covalent interaction analysis shows that the strongest H-bonds are observed near NH_2 within the favipiravir molecule. Finally, the acquired results show that the interaction of ZnO NCs with the favipiravir anticancer drug can have the potential as drug delivery carriers.

1. Introduction

The bulk zinc oxide (ZnO) and its different forms as nanostructure (nanoparticles, nanowires, nanotubes, etc.) have attracted great scrutiny in many areas including solar cells, the light-emitting/detecting diodes, gas sensors, etc. [1–9]. ZnO nanoparticles (NPs)/quantum dots (QDs), more specifically, have been significant attention because of their desirable properties such as strong adsorption capability and easily tunable surface used in important areas such as photosensors [10], electronics [11], and biomedical applications [12]. The use of ZnO NPs in biomedicine enables the treatment of different diseases such as bacterial, viral, and carcinogenic due to their remarkable properties such as biocompatibilities, their low cost, biosafety, low toxicity, and heat resistivity in comparison to other metal oxide NPs, which make them suitable for drug delivery systems [13, 14]. Also, ZnO NPs can display inherent anticancer and antimicrobial activities which makes them more excellent than other commonly used drug carriers, such as lipid and polymeric NPs [15]. Several reports address the interaction and adsorption behavior of ZnO NPs and nanoclusters (NCs) with different systems [16–21]. The interaction of $Zn_{12}O_{12}$ NCs with 6-thioguanine anticancer drug show that $Zn_{12}O_{12}$ NCs can have the potential as drug delivery carriers [22].

Many treatments including oral and injection medicines can adversely affect healthy cells and cause side and toxic effects [23]. In some cases, furthermore, it can be possible to use higher doses of a drug to get rid of an effect of disease [24]. Recent studies show that nanotechnology plays a significant role as drug delivery carriers [25] and has always made it easy to control drug-release characteristics of time course and/or location in the body [26, 27]. Most importantly, drug delivery systems can deliver a rather high amount of drug molecules and reduce possible severe side effects without producing a toxic effect [28].

In this context, the main objective of this study was to clarify the potential mechanism of possible interaction between ZnO NCs with different sizes and favipiravir anticancer drug and to figure out the potential use of ZnO NCs as a drug carrier. Herein, the electronic and energetic properties such as the adsorption energy, binding energy, density of states, UV-vis spectra, etc. were performed using density functional theory (DFT) and time-dependent DFT.

2. Computational Details

The DFT simulations were implemented to understand the interaction mechanisms of the favipiravir drug molecule with ZnO NCs (with different sizes) along with B3LYP functional with the 6-31G(d) basis set [29] and Grimme's three-parameter which is an empirical dispersion correction [30]. To get the possible interactions of the favipiravir drug molecule with ZnO NCs, the favipiravir and ZnO NCs, firstly, were optimized and later the structures with the lowest total

energy $\left(E_T\right)$ were considered. All calculations were carried out using Gaussian 09 [31]. To calculate the adsorption energy $\left(E_{ad}\right)$ of favipiravir drug and ZnO NCs interactions, the following expression is used:

$$E_{ad} = E(NC + Drug) - E(NC) - E(Drug) + E(BSSE) \quad (1)$$

where $E(NC + Drug)$ is the total energy (E_T) of the interacting systems. $E(NC)$ and $E(Drug)$ are the E_T of isolated NCs and favipiravir, respectively. $E(BSSE)$ is known as the "basis set superposition error", which is calculated by the counterpoise method to obtain highly accurate energy prediction [32].

On the other hand, the vertical ionization potential (VIP) and vertical electron affinity (VEA) are performed using [$VIP = E^{cation} - E^{neutral}$] and [$VEA = E^{neutral} - E^{anion}$] where the VIP is the energy difference between the ground state (GS) of the cation $\left(E^{cation}\right)$ and the GS of the neutral $\left(E^{neutral}\right)$ at the geometry of the neutral. VEA is the energy difference between the GS of the neutral and the GS of the anion $\left(E^{anion}\right)$ at the geometry of the neutral. Moreover, the Wiberg bond index (WBI), Fuzzy bond orders (FBO) and Mayer bond order (MBO) are performed using the Multiwfn program [33]. The TD-DFT calculations based on CAM-B3LYP functional [34] with 6-31G(d) basis set is applied for guessing UV – vis spectra.

3. Results And Discussions

The structures, electronic states, and point group symmetries of pure $(ZnO)_{12}$, $(ZnO)_{15}$, $(ZnO)_{18}$, $(ZnO)_{20}$, $(ZnO)_{22}$, and $(ZnO)_{24}$ NCs are optimized and represented in Fig. 1. The $(ZnO)_{12}$ and $(ZnO)_{18}$ NCs are found to be the potential energy surface (PES) of the ^1A_G state, the $(ZnO)_{15}$ NC is the ground $^1A'$ singlet PES. The $(ZnO)_{20}$, $(ZnO)_{22}$, and $(ZnO)_{24}$ NCs are found to be the PES of the ^1A state. The point group symmetries of $(ZnO)_{12}$, $(ZnO)_{15}$, $(ZnO)_{18}$, $(ZnO)_{20}$, $(ZnO)_{22}$, and $(ZnO)_{24}$ NCs are T_h, C_{3h}, S_6, C_{4h}, C_3 and $S_{8,}$ respectively. From the harmonic vibrational frequencies, the studied ZnO NC models corresponded to energetic a minimum which means the transition state at a saddle-point on the PES.

All possible interactions of the $(ZnO)_{12}$, $(ZnO)_{15}$, $(ZnO)_{18}$, $(ZnO)_{20}$, $(ZnO)_{22}$, and $(ZnO)_{24}$ NCs with favipiravir drug were carried out and among them, relaxed structures with the lowest energy are demonstrated in Fig. 2. The binding energy per atom $\left(E_b\right)$ of pure ZnO NCs and adsorption energy $\left(E_{ad}\right)$ of theoretically calculated geometries of the favipiravir adsorbed ZnO NCs are depicted in Fig. 3. The E_b of the ZnO NCs shifts from 5.04 eV to 5.16 eV, depending on the increase in the size. These results indicate that an increase in the size of the NCs also enhances the stability. The E_{ad} of the ZnO NCs are predicted in the range of -26.69 kcal/mol and – 34.27 kcal/mol where N – Zn and F – Zn atoms interact between the N and F atoms of favipiravir drug and Zn atoms of the ZnO NCs. The negative E_{ad} means the adsorption of the favipiravir drug on ZnO NCs is exothermic and energetically favorable. The size of ZnO NC has a significant effect on the E_{ad} between the favipiravir and ZnO NCs. It is important to note that the E_{ad} (-34.27 kcal/mol) of between $(ZnO)_{18}$ NC and the favipiravir is more desirable than the other interactions $(ZnO)_{24}$ (-26.69 kcal/mol), $(ZnO)_{20}$ (-27.14 kcal/mol), $(ZnO)_{12}$ (-29.36 kcal/mol), $(ZnO)_{15}$ (-29.50 kcal/mol), and $(ZnO)_{22}$ (-31.04 kcal/mol) NCs with the favipiravir, which means that ZnO NCs can be used as drug delivery vehicle.

The HOMO and LUMO energy levels are an important parameter to understand perfectly the charge transfer interaction within interacting systems [35]. In this regard, the energy levels using the density of states (DOS) constructed by GaussSum [36] (see Fig. 4) and the energy gap $\left(E_g\right)$ which is obtained from HOMO and LUMO energy difference are performed to figure out the stability chemical reaction of the studied systems. The size of ZnO NCs causes changes

over valence and conduction levels to shift to higher and lower energies both pure and interacting systems, leading to a shift in the studied systems. The value of the HOMO and LUMO energy levels are found to be about − 6.05 and − 3.28eV, respectively, and corresponding the E_g is found as 2.77 eV for $(ZnO)_{15}$ NC and the favipiravir interaction which is the smallest value among the studied models. Moreover, the HOMO and LUMO energy levels for $(ZnO)_{12}$ NC and the favipiravir interaction are predicted as -6.19 and − 3.25 eV, respectively. The corresponding $E_g$is found to be 2.94 eV, which is the greatest value than the other ZnO NC and the favipiravir interactions which change in the range of 2.85—3.94 eV. It is important to note that charge transfer can take place easier between HOMO and LUMO energy levels of $(ZnO)_{15}$ NC which has the smallest $E_g$value and the favipiravir interaction, which means a shift in the biological activity of the favipiravir and ZnO NC interaction shown in Fig. 5. That is, the change in the size of the ZnO NCs and the position of the favipiravir on the ZnO NCs cause a desirable shift in the HOMO and LUMO energy levels due to a decrease in the E_g, which further contributes to the charge-transfer process [37–39]. The percentage value $\left(\Delta E_g\right)$ of the difference in the E_g energies for favipiravir adsorbed ZnO NCs also given in Fig. 5. When compared to pure ZnO NCs, the greatest change in the ΔE_g is predicted between $(ZnO)_{12}$ NC and favipiravir (31.16%), whereas the lowest change in the ΔE_g is predicted between $ZnO)_{22}$ NC and favipiravir (18.41%). The values show that the size of ZnO NCs has an important effect on the E_g of interactions. The ZnO NCs are semi-conducting with the E_g in the range of 2.77–2.97 eV.

The vertical ionization potential (VIP) and vertical electron affinity (VEA), which are defined in computational part, are carried out to explore the changes of the reactivity properties of pure ZnO NCs and ZnO NCs with favipiravir drug based on the size of ZnO NCs, as indicated in Fig. 6 (a, b). The greater VIP value of pure $(ZnO)_{12}$ NC is 8.40 eV, which decreases to 7.84 eV for $(ZnO)_{24}$ NC due to the increase in HOMO and LUMO energy levels in terms of the electron-donating ability of the favipiravir towards ZnO NCs. Similarly, the greater VIP value of $(ZnO)_{18}$ NC with favipiravir drug is 7.53 eV, which decreases to 7.25 eV for $(ZnO)_{22}$ and $(ZnO)_{24}$ NCs with favipiravir drug as shown in Fig. 6a. It is important to note that pure $(ZnO)_{12}$ NC and $(ZnO)_{18}$ NC with favipiravir drug is more stable than that of the others so it is difficult to eject the electron from them. This result agrees also with the energy levels of HOMO and LUMO (see Table I). The VIP of the $(ZnO)_{15}$, $(ZnO)_{18}$ and $(ZnO)_{20}$ NCs with favipiravir drug are predicted as 7.29, 7.53 and 7.31 eV. The value of VEA of pure $(ZnO)_{20}$ is 2.01 eV, which decreases to 1.64 eV for pure $(ZnO)_{20}$ as shown in Fig. 6b. Similarly, the greater VEA value of $(ZnO)_{18}$ NC with favipiravir drug is 1.95 eV, which decreases to 1.57 eV for $(ZnO)_{12}$ NC with favipiravir drug as shown in Fig. 6b. There is not a smooth change for the VEA with increase in the size of ZnO NC where the value of VEA increase for $(ZnO)_{12}$, $(ZnO)_{15}$ and $(ZnO)_{18}$ with the favipiravir drug from 1.64 to 1.95 eV, and then fluctuations are observed from $(ZnO)_{20}$ to $(ZnO)_{24}$ with the favipiravir drug.

Ultraviolet-visible (UV–vis) absorption spectra of interacting pure and favipiravir adsorbed $(ZnO)_{12}$, $(ZnO)_{15}$, $(ZnO)_{18}$, $(ZnO)_{20}$, $(ZnO)_{22}$ $(ZnO)_{24}$ NCs are performed with TD-DFT, and the obtained results are piloted in Fig. 7. An excitation wavelength (electron-transfer wavelength) in the visible region is preferred because ultraviolet light is harmful to living organisms [40]. Our results show that the maximum UV–vis of ZnO NCs with different sizes and favipiravir interactions shows the peaks located wavelengths between 250 and 265 nm which corresponds to the near UV region and the closest visible light.

The bond order analysis of ZnO NCs with different sizes and favipiravir interactions was studied using Wiberg bond order (WBO), Mayer bond order (MBO) and Fuzzy bond order (FBO) methods. The values of WBI, FBO and MBO for the favipiravir on the $(ZnO)_{22}$ NC were calculated about 0.432, 0.762, and 0.402, respectively, which are greater than other configurations (see Table 2, Fig. 8, and Fig. S1 in Supporting Information). WBI, FBO and MBO values also vary considerably based on the NC size and binding points of favipiravir molecule. Bond order values below 1.0 reflect the

fact that bonds between O – Zn, N – Zn and F – Zn atoms exhibit dual covalent and ionic natures. Besides, the presence of metal ions bonded to oxygen atoms means that the O – Zn bonds are kind of polarized covalent bonds. The Mulliken charge distribution of the atoms in the ZnO NCs with different sizes and favipiravir interactions is also tabulated in Table 2 and shown in Fig. S1 (in Supporting Information). As can be seen from Table 2, the positive charge of the O – Zn interactions has been calculated between 0.304 and 0.360 |e| which are significantly bigger than the other positive charges of N – Zn and F – Zn interactions.

Table 1
The calculated binding energy per atom (E_b), adsorption energy (E_{ad}), vertical ionization potential (VIP), vertical electron affinity (VEA), HOMO and LUMO energies, band gap energy (E_g) and reactivity parameters for pure and favipiravir adsorbed ZnO NCs. E_{ad} in kcal/mol. Electronic properties are described in eV.

	$(ZnO)_{12}$		$(ZnO)_{15}$		$(ZnO)_{18}$		$(ZnO)_{20}$		$(ZnO)_{22}$		$(ZnO)_{24}$	
	Pure	**Ads.**	**Pure**	**Ads.**	**Pure**	**Ads.**	**Pure**	**Ads.**	**Pure**	**Ads.**	**Pure**	**Ads.**
E_b	5.04	-	5.08	-	5.11	-	5.13	-	5.15	-	5.16	-
E_{ad}	-	-29.36	-	-29.50	-	-34.27	-	-27.14	-	-31.04	-	-26.69
VIP	8.40	7.46	8.13	7.29	8.03	7.53	7.99	7.31	7.80	7.25	7.84	7.25
VEA	1.64	1.57	1.79	1.67	1.90	1.95	1.87	1.76	2.01	1.86	1.97	1.85
LUMO	-2.86	-3.27	-2.92	-3.28	-2.96	-3.47	-2.90	-3.25	-3.01	-3.22	-2.92	-3.27
HOMO	-7.00	-6.12	-6.85	-6.05	-6.87	-6.38	-6.84	-6.19	-6.65	-6.19	-6.80	-6.20
E_g	4.14	2.85	3.93	2.77	3.91	2.91	3.94	2.94	3.64	2.97	3.88	2.93
$\Delta E_g(\%)$*	-	31.16	-	29.52	-	25.58	-	25.38	-	18.41	-	24.48
η	2.07	1.43	1.97	1.39	1.96	1.46	1.97	1.47	1.82	1.49	1.94	1.47
ΔN_{tot}	2.38	3.29	2.49	3.37	2.51	3.38	2.47	3.21	2.65	3.17	2.51	3.23

*$\Delta E_g(\%)$ denotes the changes after adsorption.

Table 2
Bond orders (Wiberg bond index; WBI, Fuzzy bond order; FBO, Mayer bond order; MBO) and Mulliken charges based on interactions between O – Zn, N – Zn and F – Zn atoms (The O, N, and F atoms indicate favipiravir, the Zn is the closest neighbors to these atoms; see Supporting Information Fig. S1 for detail).

Configurations	Interactions	WBI	FBO	MBO	Charge
Drug – $(ZnO)_{12}$	27O — 19Zn	0.414	0.732	0.363	0.321
	35N — 19Zn	0.189	0.369	0.115	0.072
	34F — 6Zn	0.056	0.105	0.072	0.064
Drug – $(ZnO)_{15}$	33O — 30Zn	0.415	0.732	0.365	0.325
	41N — 30Zn	0.195	0.378	0.117	0.074
	40F — 7Zn	0.031	0.041	0.042	0.039
Drug – $(ZnO)_{18}$	39O — 25Zn	0.370	0.675	0.334	0.304
	47N — 9Zn	0.373	0.636	0.259	0.241
	46F — 9Zn	0.042	0.079	0.087	0.085
Drug – $(ZnO)_{20}$	43O — 19Zn	0.426	0.750	0.409	0.358
	51N — 19Zn	0.089	0.167	0.061	0.061
	50F — 16Zn	0.145	0.312	0.187	0.169
Drug – $(ZnO)_{22}$	47O — 33Zn	0.432	0.762	0.402	0.360
	55N — 33Zn	0.067	0.119	0.029	0.033
	54F — 25Zn	0.175	0.371	0.229	0.199
Drug – $(ZnO)_{24}$	51O — 16Zn	0.405	0.725	0.370	0.338
	59N — 16Zn	0.172	0.338	0.092	0.053
	58F — 22Zn	0.041	0.060	0.045	0.040

To get an insight into the non-covalent interactions (NCI) within the studied systems, the NCI isosurfaces for favipiravir adsorbed $(ZnO)_{12}$, $(ZnO)_{15}$, $(ZnO)_{18}$, $(ZnO)_{20}$, $(ZnO)_{22}$, $(ZnO)_{24}$ NCs are investigated and plots for studied systems are shown in Fig. 9. As can be seen, disk-shaped blocks that indicate non-covalent interactions and the strongest H-bonds are observed near NH_2 within the favipiravir molecule. Furthermore, the reduced density gradient (RDG) scatter plots for favipiravir adsorbed ZnO NCs were presented in Fig. 10. RDG scattered points indicate H-bonding interactions on the negative scale (blue color), indicating the dominance of the effect of strong attractive interactions. The green region in the range of $\rho = 0.00$ and $\rho = -0.02$ also shows the dominance of the effect of Van der Waals forces between binding atoms. Red areas indicate strong repulsive/steric interactions in a range of 0.01 and 0.05.

4. Conclusions

In this study, the adsorption behavior and electronic and structural properties of the interacting favipiravir drug and ZnO NCs with different sizes using the DFT method. Our results show the size of ZnO NCs, and binding points have an important effect on the interactions. For example, the adsorption energy between $(ZnO)_{18}$ NC and the favipiravir (-34.27

kcal/mol) is energetically more favorable than the other interactions. The size of the ZnO NCs causes a decrease in the energy gap, which further contributes to the charge-transfer process. The bonds between O – Zn, N – Zn and F – Zn atoms exhibit dual covalent and ionic natures. From the non-covalent interaction analysis, the strongest H-bonds are observed near NH_2 within the favipiravir. The maximum absorption peaks are predicted in the near UV region and the closest visible light. We can conclude that the ZnO NCs can have potential as drug delivery carriers.

Declarations

Acknowledgments

The numerical calculations reported were partially performed at TUBITAK ULAKBIM, High Performance and Grid Computing Centre (TRUBA resources), Turkey.

Compliance with Ethical Standards

This article does not contain any studies involving human participants performed by any of the authors.

Competing Interests

The authors declare that they have no conflicts of interest.

Research Data Policy and Data Availability Statements

Data sharing not applicable to this article as no datasets were generated or analysed during the current study.

Author Contribution

Mustafa Kurban: Supervision, Investigation, Conceptualization, Writing- original draft, Writing- review & editing, Data curation, Validation, Software.

İskender Muz: Investigation, Project administration, Visualization, Methodology, Conceptualization, Writing- original draft, Writing- review & editing, Data curation, Software.

References

1. J. Wager, B. Yeh, R. Hoffman, D.K.-C.O. in S. State, U. 2014, An amorphous oxide semiconductor thin-film transistor route to oxide electronics, Curr. Opin. Solid State Mater. Sci. 18 (2014) 53–61.
2. M. Laurenti, G. Canavese, S. Stassi, … M.F.-R., U. 2016, A porous nanobranched structure: An effective way to improve piezoelectricity in sputtered ZnO thin films, RSC Adv. 6 (2016) 76996–77004.
3. J. Liu, M. V. Fernández-Serra, P.B. Allen, First-principles study of pyroelectricity in GaN and ZnO, Phys. Rev. B. 93 (2016) 081205. https://doi.org/10.1103/PHYSREVB.93.081205/FIGURES/5/MEDIUM.
4. R.Q. Song, A.W. Xu, B. Deng, Q. Li, G.Y. Chen, From Layered Basic Zinc Acetate Nanobelts to Hierarchical Zinc Oxide Nanostructures and Porous Zinc Oxide Nanobelts, Adv. Funct. Mater. 17 (2007) 296–306. https://doi.org/10.1002/ADFM.200600024.
5. P. Hu, Y. Liu, X. Wang, L. Fu, D. Zhu, Tower-like structure of ZnO nanocolumns, Chem. Commun. 11 (2003) 1304–1305. https://doi.org/10.1039/B302821F.
6. J. Zhang, L. Sun, C. Liao, C. Yan, A simple route towards tubular ZnO, Chem. Commun. 2 (2002) 262–263. https://doi.org/10.1039/B108863G.

7. S. Polarz, A. V Orlov, F. Schüth, A.-H. Lu, S. Polarz, A. V Orlov, F. Schüth, A.-H. Lu, Preparation of high-surface-area zinc oxide with ordered porosity, different pore sizes, and nanocrystalline walls, Kops.Uni-Konstanz.De. 13 (2007) 592–597. https://doi.org/10.1002/chem.200600428.
8. X.Y. Kong, Y. Ding, R. Yang, Z.L. Wang, Single-Crystal Nanorings Formed by Epitaxial Self-Coiling of Polar Nanobelts, Science (80-.). 303 (2004) 1348–1351.
9. X. Zhong, W. Knoll, Morphology-controlled large-scale synthesis of ZnO nanocrystals from bulk ZnO, Chem. Commun. (2005) 1158–1160. https://doi.org/10.1039/B414948C.
10. S.P. Chang, K.J. Chen, Zinc oxide nanoparticle photodetector, J. Nanomater. 2012 (2012). https://doi.org/10.1155/2012/602398.
11. A. Kołodziejczak-Radzimska, T.J.- Materials, undefined 2014, Zinc oxide—from synthesis to application: a review, Mdpi.Com. 7 (2014) 2833–2881. https://doi.org/10.3390/ma7042833.
12. Y. Zhang, T. Nayak, … H.H.-C. molecular, U. 2013, Biomedical applications of zinc oxide nanomaterials, Curr. Mol. Med. 13 (2013) 1633–1645.
13. J.W. Rasmussen, E. Martinez, P. Louka, D.G. Wingett, Zinc oxide nanoparticles for selective destruction of tumor cells and potential for drug delivery applications, Expert Opin. Drug Deliv. 7 (2010) 1063–1077. https://doi.org/10.1517/17425247.2010.502560.
14. H.-M. Xiong, H.-M. Xiong, ZnO Nanoparticles Applied to Bioimaging and Drug Delivery, Adv. Mater. 25 (2013) 5329–5335. https://doi.org/10.1002/ADMA.201301732.
15. S. Saha, P. Sarkar, Understanding the interaction of DNA-RNA nucleobases with different ZnO nanomaterials, Phys. Chem. Chem. Phys. 16 (2014) 15355–15366. https://doi.org/10.1039/C4CP01041H.
16. V.L. Chandraboss, B. Karthikeyan, S. Senthilvelan, Experimental and first-principles study of guanine adsorption on ZnO clusters, Phys. Chem. Chem. Phys. 16 (2014) 23461–23475. https://doi.org/10.1039/C4CP03274H.
17. X. Yang, X. Zhang, Z. Liu, Y. Ma, Y. Huang, Y. Chen, High-efficiency loading and controlled release of doxorubicin hydrochloride on graphene oxide, J. Phys. Chem. C. 112 (2008) 17554–17558. https://doi.org/10.1021/JP806751K.
18. N.F. Rosli, M. Fojtů, A.C. Fisher, M. Pumera, Graphene Oxide Nanoplatelets Potentiate Anticancer Effect of Cisplatin in Human Lung Cancer Cells, Langmuir. 35 (2019) 3176–3182. https://doi.org/10.1021/ACS.LANGMUIR.8B03086.
19. M. Baek, H.E. Chung, J. Yu, J.A. Lee, T.H. Kim, J.M. Oh, W.J. Lee, S.M. Paek, J.K. Lee, J. Jeong, J.H. Choy, S.J. Choi, Pharmacokinetics, tissue distribution, and excretion of zinc oxide nanoparticles, Int. J. Nanomedicine. 7 (2012) 3081. https://doi.org/10.2147/IJN.S32593.
20. S.J. Choi, J.H. Choy, Biokinetics of zinc oxide nanoparticles: toxicokinetics, biological fates, and protein interaction, Int. J. Nanomedicine. 9 (2014) 261. https://doi.org/10.2147/IJN.S57920.
21. W. Xu, H. Cao, H. Chen, Y. Yang, A. Sarkar, Sensing the cathinone drug concentration in the human body by using zinc oxide nanostructures: a DFT study, Struct. Chem. 32 (2021) 63–68. https://doi.org/10.1007/s11224-020-01611-y.
22. X. Ji, S. Jameh-Bozorghi, Metal oxide nanoclusters as drug delivery systems for an anticancer drug: a theoretical study, Mol. Phys. 118 (2020). https://doi.org/10.1080/00268976.2020.1738581.
23. L. Bai, X. Li, L. He, Y. Zheng, H. Lu, J. Li, L. Zhong, R. Tong, Z. Jiang, J. Shi, J. Li, Antidiabetic Potential of Flavonoids from Traditional Chinese Medicine: A Review, Am. J. Chin. Med. 47 (2019) 933–957. https://doi.org/10.1142/S0192415X19500496.
24. P. Sharma, D.G.I. Scott, Optimizing Methotrexate Treatment in Rheumatoid Arthritis: The Case for Subcutaneous Methotrexate Prior to Biologics, Drugs. 75 (2015) 1953–1956. https://doi.org/10.1007/s40265-015-0486-7.

25. M. Kurban, İ. Muz, Theoretical investigation of the adsorption behaviors of fluorouracil as an anticancer drug on pristine and B-, Al-, Ga-doped C36 nanotube, J. Mol. Liq. 309 (2020) 113209. https://doi.org/10.1016/j.molliq.2020.113209.
26. B. Khezri, S.M.B. Mousavi, L. Krejcova, Z. Heger, Z. Sofer, M. Pumera, Ultrafast Electrochemical Trigger Drug Delivery Mechanism for Nanographene Micromachines, Adv. Funct. Mater. 29 (2019). https://doi.org/10.1002/adfm.201806696.
27. S. Campuzano, B. Esteban-Fernández De Ávila, P. Yáñez-Sedeño, J.M. Pingarrón, J. Wang, Nano/microvehicles for efficient delivery and (bio)sensing at the cellular level, Chem. Sci. 8 (2017) 6750–6763. https://doi.org/10.1039/c7sc02434g.
28. L.J. Sham, W. Kohn, One-particle properties of an inhomogeneous interacting electron gas, Phys. Rev. 145 (1966) 561–567. https://doi.org/10.1103/PHYSREV.145.561.
29. A.D. Becke, A new mixing of hatree-fock and local density functional theories, J. Chem. Phys. 98 (1993) 1372–1377. https://doi.org/10.1063/1.464304.
30. S. Grimme, S. Ehrlich, L. Goerigk, Effect of the Damping Function in Dispersion Corrected Density Functional Theory, J. Comput. Chem. 32 (2011) 1456–1465. https://doi.org/10.1002/jcc.21759.
31. M.J. Frisch, G.W. Trucks, H.B. Schlegel, G.E. Scuseria, M.A. Robb, J.R. Cheeseman, G. Scalmani, V. Barone, B. Mennucci, G.A. Petersson, H. Nakatsuji, M. Caricato, X. Li, H.P. Hratchian, A.F. Izmaylov, J. Bloino, G. Zheng, J.L. Sonnenberg, M. Hada, M. Ehara, K. Toyota, R. Fukuda, J. Hasegawa, M. Ishida, T. Nakajima, Y. Honda, O. Kitao, H. Nakai, T. Vreven, J.A. Montgomery, J.E. Peralta, F. Ogliaro, M. Bearpark, J.J. Heyd, E. Brothers, K.N. Kudin, V.N. Staroverov, R. Kobayashi, J. Normand, K. Raghavachari, A. Rendell, J.C. Burant, S.S. Iyengar, J. Tomasi, M. Cossi, N. Rega, J.M. Millam, M. Klene, J.E. Knox, J.B. Cross, V. Bakken, C. Adamo, J. Jaramillo, R. Gomperts, R.E. Stratmann, O. Yazyev, A.J. Austin, R. Cammi, C. Pomelli, J.W. Ochterski, R.L. Martin, K. Morokuma, V.G. Zakrzewski, G.A. Voth, P. Salvador, J.J. Dannenberg, S. Dapprich, A.D. Daniels, Farkas, J.B. Foresman, J. V Ortiz, J. Cioslowski, D.J. Fox, Gaussian 09, Revision E.01, Gaussian Inc., Wallingford CT. (2009).
32. S.F. Boys, F. Bernardi, The calculation of small molecular interactions by the differences of separate total energies. Some procedures with reduced errors, Mol. Phys. 19 (1970) 553–566. https://doi.org/10.1080/00268977000101561.
33. T. Lu, F. Chen, Multiwfn: A multifunctional wavefunction analyzer, J. Comput. Chem. 33 (2012) 580–592. https://doi.org/10.1002/jcc.22885.
34. T. Yanai, D.P. Tew, N.C. Handy, A new hybrid exchange–correlation functional using the Coulomb-attenuating method (CAM-B3LYP), Chem. Phys. Lett. 393 (2004) 51–57. https://doi.org/10.1016/j.cplett.2004.06.011.
35. M. Zaboli, H. Raissi, The analysis of electronic structures, adsorption properties, NBO, QTAIM and NMR parameters of the adsorbed hydrogen sulfide on various sites of the outer surface of aluminum phosphide nanotube: a DFT study, Struct. Chem. 26 (2015) 1059–1075. https://doi.org/10.1007/s11224-015-0563-2.
36. N.M. O'Boyle, A.L. Tenderholt, K.M. Langner, cclib: A library for package-independent computational chemistry algorithms, J. Comput. Chem. 29 (2008) 839–845. https://doi.org/10.1002/jcc.20823.
37. M.A. Salem, K.P. Katin, S. Kaya, A.I. Kochaev, M.M. Maslov, Interaction of dopants and functional groups adsorbed on the carbon fullerenes: Computational study, Phys. E-LOW-DIMENSIONAL Syst. NANOSTRUCTURES. 124 (2020). https://doi.org/10.1016/j.physe.2020.114319.
38. N.R. Abdullah, H.O. Rashid, M.T. Kareem, C.-S. Tang, A. Manolescu, V. Gudmundsson, Effects of bonded and non-bonded B/N codoping of graphene on its stability, interaction energy, electronic structure, and power factor, Phys. Lett. A. 384 (2020). https://doi.org/10.1016/j.physleta.2020.126350.

39. N.R. Abdullah, H.O. Rashid, C.-S. Tang, A. Manolescu, V. Gudmundsson, Modeling electronic, mechanical, optical and thermal properties of graphene-like BC6N materials: Role of prominent BN-bonds, Phys. Lett. A. 384 (2020). https://doi.org/10.1016/j.physleta.2020.126807.
40. S.C. Burdette, S.J. Lippard, ICCC34 - golden edition of coordination chemistry reviews. Coordination chemistry for the neurosciences, Coord. Chem. Rev. 216 (2001) 333–361. https://doi.org/10.1016/S0010-8545(01)00308-3.

Figures

Figure 1

(Colour online) The optimized structures, electronic states and point group symmetries of pure **(a)** $(ZnO)_{12}$, **(b)** $(ZnO)_{15}$, **(c)** $(ZnO)_{18}$, **(d)** $(ZnO)_{20}$, **(e)** $(ZnO)_{22}$, **(f)** $(ZnO)_{24}$ NCs (Gray; Zn, Red; O).

Figure 2

(Colour online) Relaxed structures for favipiravir adsorbed **(a)** $(ZnO)_{12}$, **(b)** $(ZnO)_{15}$, **(c)** $(ZnO)_{18}$, **(d)** $(ZnO)_{20}$, **(e)** $(ZnO)_{22}$, **(f)** $(ZnO)_{24}$ NCs.

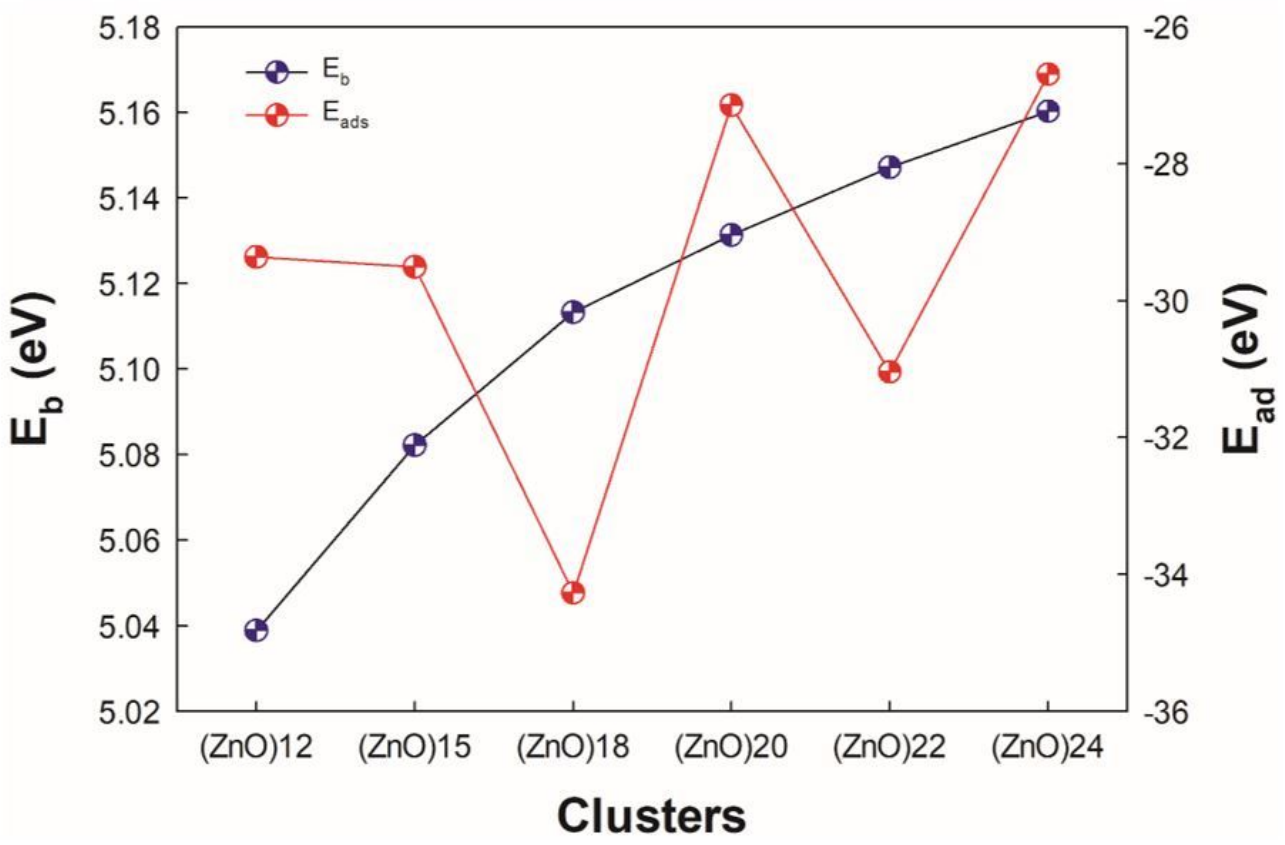

Figure 3

(Colour online) Binding energy per atom (E_b)of pure ZnO clusters and adsorption energy (E_{ad}) for favipiravir adsorbed ZnO NCs.

Figure 4

(Colour online) Density of states (DOS) for pure and favipiravir adsorbed **(a)** $(ZnO)_{12}$, **(b)** $(ZnO)_{15}$, **(c)** $(ZnO)_{18}$, **(d)** $(ZnO)_{20}$, **(e)** $(ZnO)_{22}$, **(f)** $(ZnO)_{24}$ NCs.

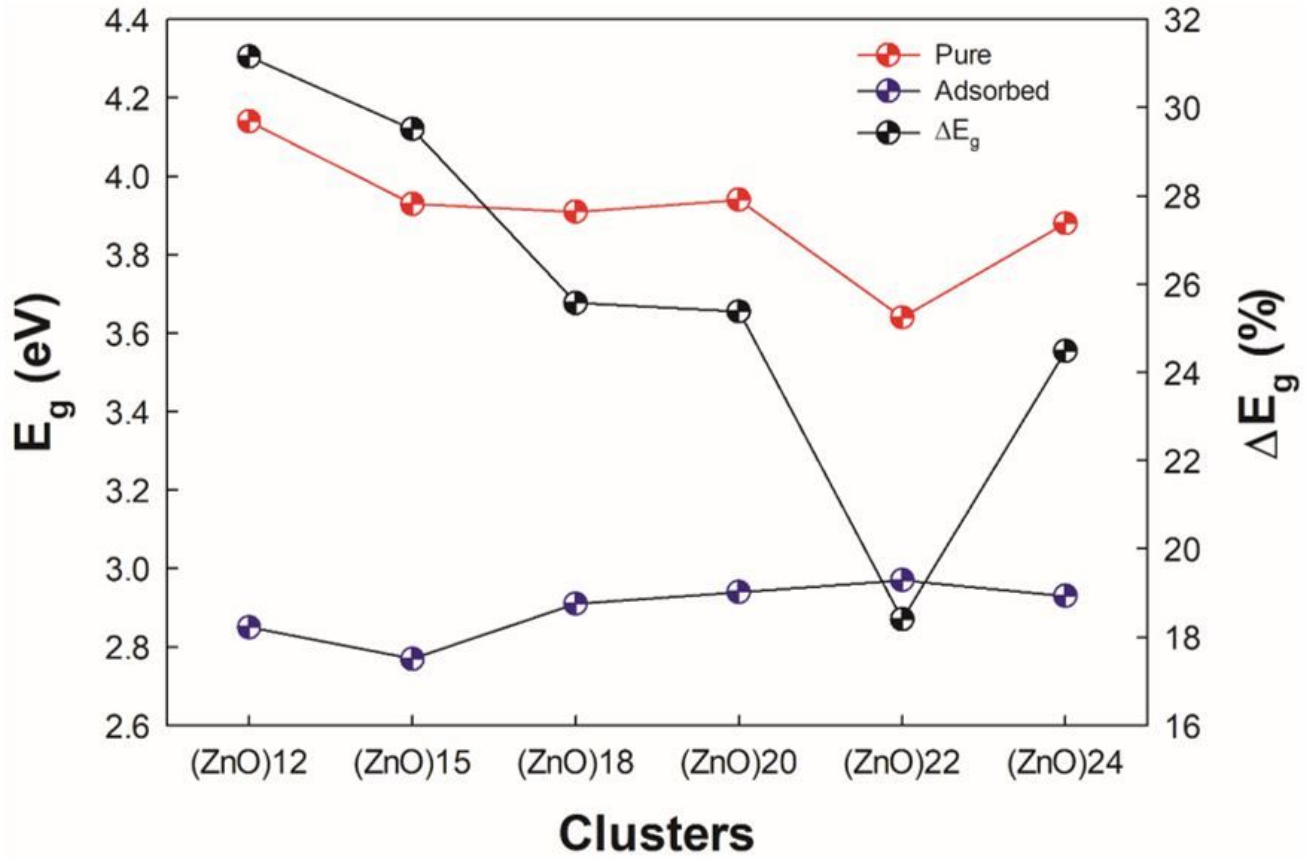

Figure 5

(Colour online) The HOMO-LUMO energy gap *(E_g)* and the percentage value *(ΔE_g)* of the difference in the E_g energies for pure and favipiravir adsorbed ZnO NCs.

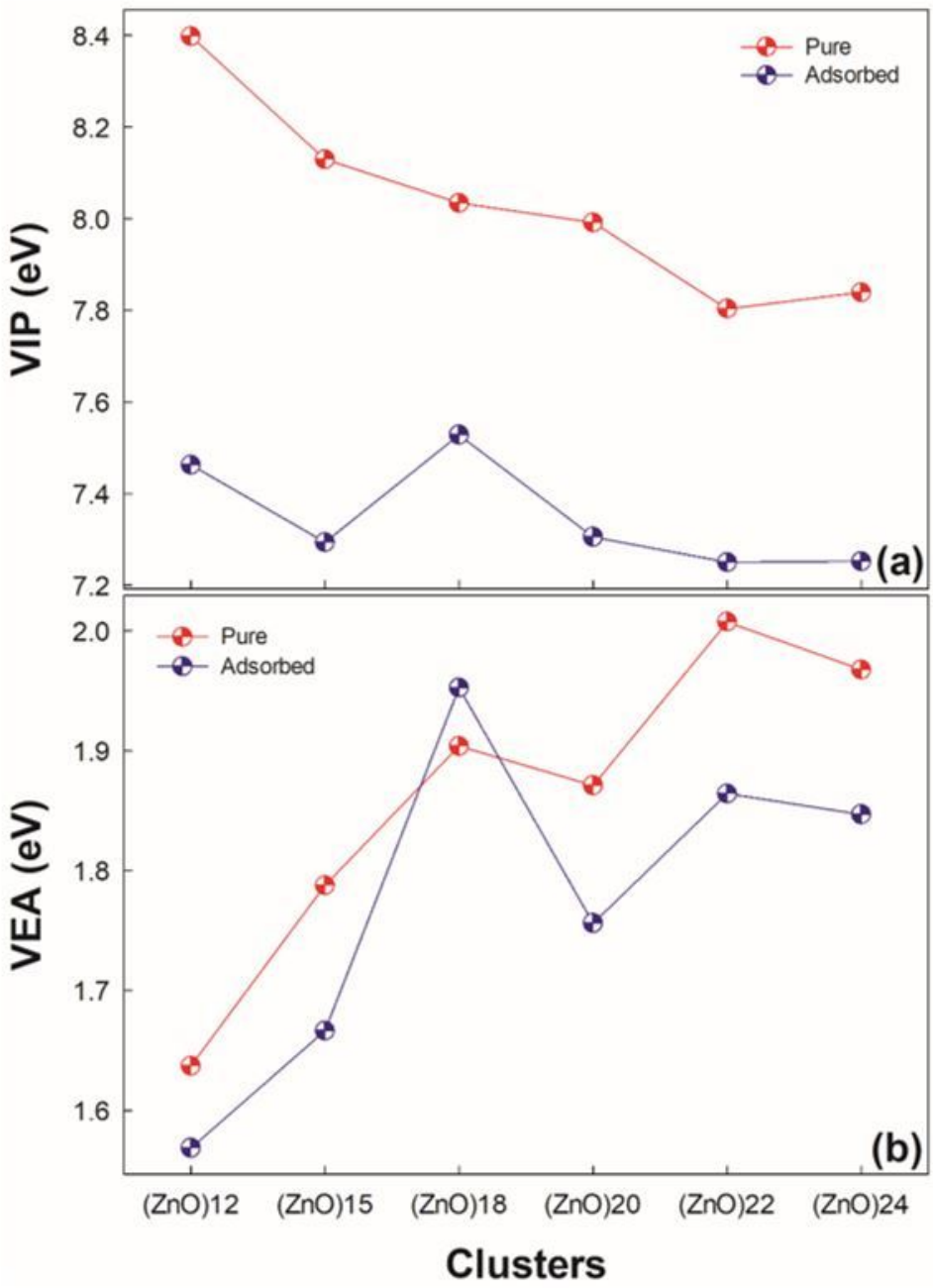

Figure 6

(Colour online) **(a)** VIP and **(b)** VEA for pure and favipiravir adsorbed ZnO NCs.

Figure 7

(Colour online) UV-vis spectra for pure and favipiravir adsorbed **(a)** $(ZnO)_{12}$, **(b)** $(ZnO)_{15}$, **(c)** $(ZnO)_{18}$, **(d)** $(ZnO)_{20}$, **(e)** $(ZnO)_{22}$, **(f)** $(ZnO)_{24}$ NCs.

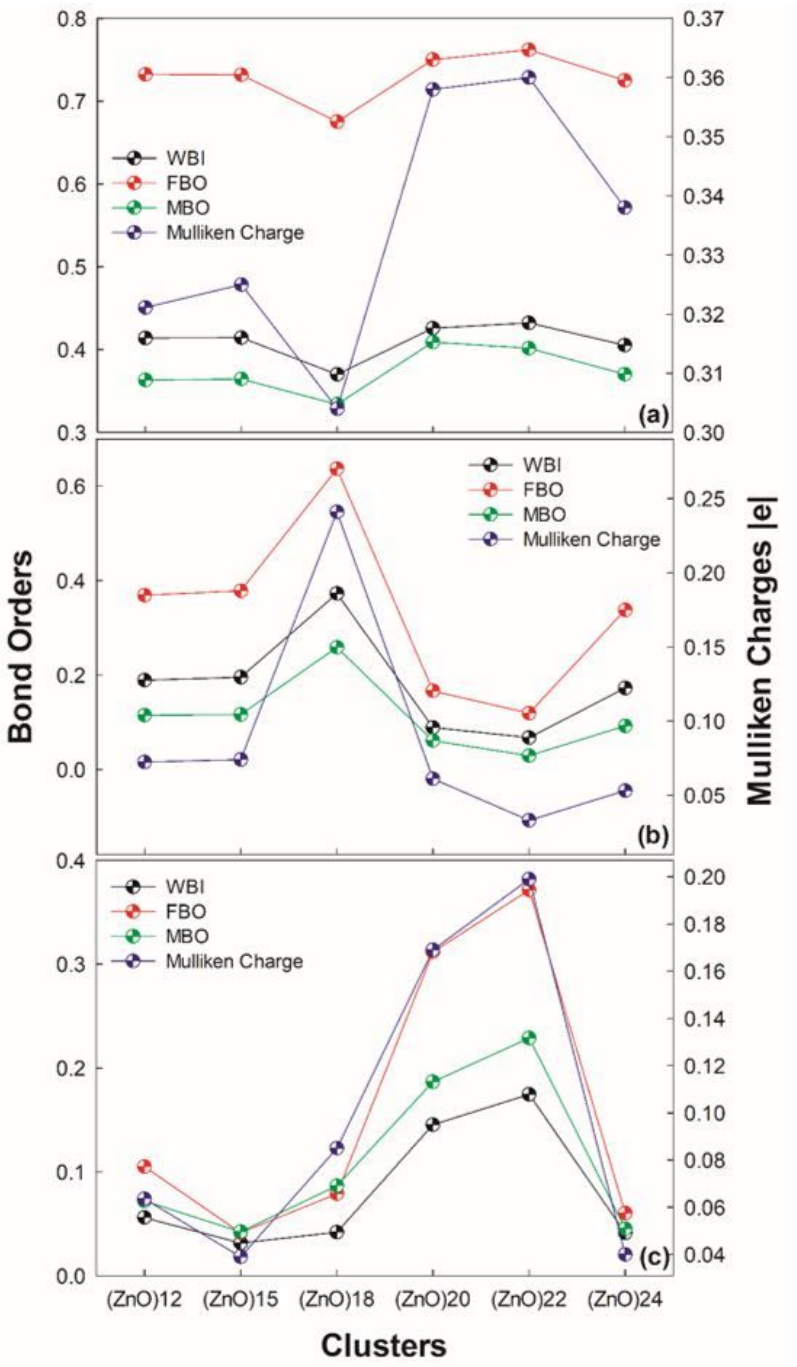

Figure 8

(Colour online) Wiberg bond index (WBO), Mayer bond order (MBO) and Fuzzy bond order (FBO) and Mulliken charges based on interactions between **(a)** O – Zn, **(b)** N – Zn and **(c)** F – Zn atoms for favipiravir adsorbed ZnO NCs (O, N and F atoms indicate favipiravir and Zn indicate ZnO NCs; according to Supporting Information Fig. S1 for detail).

Figure 9

(Colour online) The non-covalent interaction (NCI) isosurfaces for favipiravir adsorbed **(a)** $(ZnO)_{12}$, **(b)** $(ZnO)_{15}$, **(c)** $(ZnO)_{18}$, **(d)** $(ZnO)_{20}$, **(e)** $(ZnO)_{22}$, **(f)** $(ZnO)_{24}$ NCs.

Figure 10

(Colour online) The reduced density gradient (RDG) scatter plots for favipiravir adsorbed **(a)** $(ZnO)_{12}$, **(b)** $(ZnO)_{15}$, **(c)** $(ZnO)_{18}$, **(d)** $(ZnO)_{20}$, **(e)** $(ZnO)_{22}$, **(f)** $(ZnO)_{24}$ NCs. Blue represents strong attractive interactions; green indicates van der Waals interactions and red indicates repulsive/steric interactions.

Supplementary Files

This is a list of supplementary files associated with this preprint. Click to download.

- Supplementary.docx